

Published in final edited form as:

*Nature*. 2015 June 11; 522(7555): 236–239. doi:10.1038/nature14503.

## ESCRT-III controls nuclear envelope reformation

Yolanda Olmos<sup>1</sup>, Lorna Hodgson<sup>2</sup>, Judith Mantell<sup>2,3</sup>, Paul Verkade<sup>2,3,4</sup>, and Jeremy G Carlton<sup>1,\*</sup>

<sup>1</sup>Division of Cancer Studies, Section of Cell Biology and Imaging King's College London London SE1 1UL

<sup>2</sup>School of Biochemistry University of Bristol Medical Sciences Building University Walk Bristol BS8 1TD

<sup>3</sup>Wolfson Bioimaging Facility University of Bristol Medical Sciences Building University Walk Bristol BS8 1TD

<sup>4</sup>School of Physiology & Pharmacology University of Bristol Medical Sciences Building University Walk Bristol BS8 1TD

### Abstract

During telophase, the nuclear envelope (NE) reforms around daughter nuclei to ensure proper segregation of nuclear and cytoplasmic contents<sup>1-4</sup>. NE reformation requires the coating of chromatin by membrane derived from the Endoplasmic Reticulum and a subsequent annular fusion step to ensure the formed envelope is sealed<sup>1,2,4,5</sup>. How annular fusion is accomplished is unknown, but it is thought to involve the p97 AAA-ATPase complex and bears a topological equivalence to the membrane fusion event that occurs during the abscission phase of cytokinesis<sup>1,6</sup>. We find here that the Endosomal Sorting Complex Required for Transport-III (ESCRT-III) machinery localises to sites of annular fusion in the forming NE and is necessary for proper post-mitotic nucleocytoplasmic compartmentalisation. The ESCRT-III component Charged Multivesicular Body Protein (CHMP) 2A is directed to the forming NE through binding to CHMP4B and provides an activity essential for NE reformation. Localisation also requires the p97 complex member Ubiquitin Fusion and Degradation 1 (UFD1). Our results describe a novel role for the ESCRT-machinery in cell division and demonstrate a conservation of the machineries involved in topologically equivalent mitotic membrane remodeling events.

### Keywords

Cell Biology; Mitosis; ESCRT; Nuclear Envelope; Cell Division

---

Users may view, print, copy, and download text and data-mine the content in such documents, for the purposes of academic research, subject always to the full Conditions of use:[http://www.nature.com/authors/editorial\\_policies/license.html#terms](http://www.nature.com/authors/editorial_policies/license.html#terms)

\*Correspondence : Jeremy.Carlton@kcl.ac.uk.

Author Contributions

JGC conceived the study. PV, LH and JM designed, performed and analysed electron microscopy experiments. JGC and YO designed, performed and analysed data from other experiments. JGC wrote the manuscript with assistance from all other authors.

The ESCRT-III complex performs a topologically unique membrane fusion, allowing release of enveloped retroviruses during viral budding, intraluminal vesicles during multivesicular body biogenesis, and daughter cells during the abscission phase of cytokinesis<sup>7-11</sup>. We found that as well as localising to the midbody during late cytokinesis, endogenous ESCRT-III components CHMP2A and CHMP2B encircled the forming daughter nuclei during telophase (Figure 1A, 1B and Extended Data Figure 1A). CHMP2A localisation was sensitive to CHMP2A-targeting siRNA (Extended Data Figure 1B) and was not continuous; rather we found that CHMP2A adopted a transient punctate localisation around the decondensing nuclei during telophase (Extended Data Figure 1C, Supplementary Video 1). By scoring localisation in HeLa cells stably expressing mCh-tubulin, (cell cycle of  $21.5 \pm 1.7$  hours,  $n = 93$ ), we estimate the duration of CHMP2A localisation to be  $96 \pm 8.9$  seconds. We found cells expressing GFP-CHMP4B<sup>12</sup> also displayed a transient, punctate, juxta-nuclear localisation during telophase with recruitment of GFP-CHMP4B lasting  $225 \pm 66$  seconds ( $n = 8$ ,  $\pm$  S.D.) and individual puncta lasting  $75 \pm 46$  seconds ( $n = 92$ ,  $\pm$  S.D., Extended Data Figure 1D, Supplementary Video 2). Telophase ESCRT-III localisation was observed in other cell lines, including human-diploid fibroblasts (Extended Data Figure 1E). Using HeLa cells stably expressing a Yellow Fluorescence Protein (YFP)-tagged nuclear envelope marker (Lamin Associated Protein 2 $\beta$ , YFP-LAP2 $\beta$ )<sup>13</sup>, we determined that the juxtannuclear localisation corresponded to the forming nuclear envelope. Here, we observed colocalisation with the Lamin B Receptor (LBR)<sup>14</sup> (Figure 1C) and demonstrated that CHMP2A localisation occurred prior to appreciable formation of a nuclear lamina or nuclear pore complexes (Extended Data Figure 1F and 1G). Whilst mitotic chromatin association of ESCRT-III has been previously reported<sup>15</sup>, its function remains unknown. To investigate the role of ESCRT-components at the NE, we employed siRNA to deplete these proteins<sup>16</sup>. As described previously<sup>17</sup>, depletion of ESCRT-components produced aberrant nuclei and these defects phenocopied those produced by depletion of proteins required for NE reformation (Extended Data Figure 1H)<sup>18</sup>. NE-reformation is thought to be a two-phase process, separable into membrane fusion events that create an expanding reticular network with subsequent annular fusion of holes within this network to create a sealed barrier<sup>1</sup>. We next employed correlative light-electron microscopy (Extended Data Figure 2A-D) to examine telophase ESCRT-III NE-localisation. We found that at the stage of ESCRT-III recruitment, the NE had incompletely formed (Figure 1D). Two populations of CHMP2A-positive membranes were found. Firstly, isolated CHMP2A-decorated vesicles were observed in the cytoplasm, proximal to the forming NE ( $5.7 \pm 4.2$  % of total cellular gold, Extended Data Figure 2Ei). Secondly, CHMP2A-decorated double-membrane sheets were observed to coat the chromatin ( $51 \pm 1.7$  % of total cellular gold was within 100 nm of the NE). On these sheets, CHMP2A localised to discrete regions, with intact NE being devoid of label, but with CHMP2A preferentially (Extended Data Figure 2H) decorating nucleo-cytoplasmic channels (mean diameter  $38.4 \pm 12.5$  nm ( $n = 2 \pm$  S.E.M., from 17 determinations)) between the forming double membranes of the NE (Figure 1D, Extended Data Figure 2D-2G, Extended Data Figure 3A-D, Supplementary Videos 3 and 4). These channels must be resolved through annular fusion and given the observed localisation and topological equivalence with cytokinetic abscission (Figure 1E), we speculated that ESCRT-III might be involved in this process.

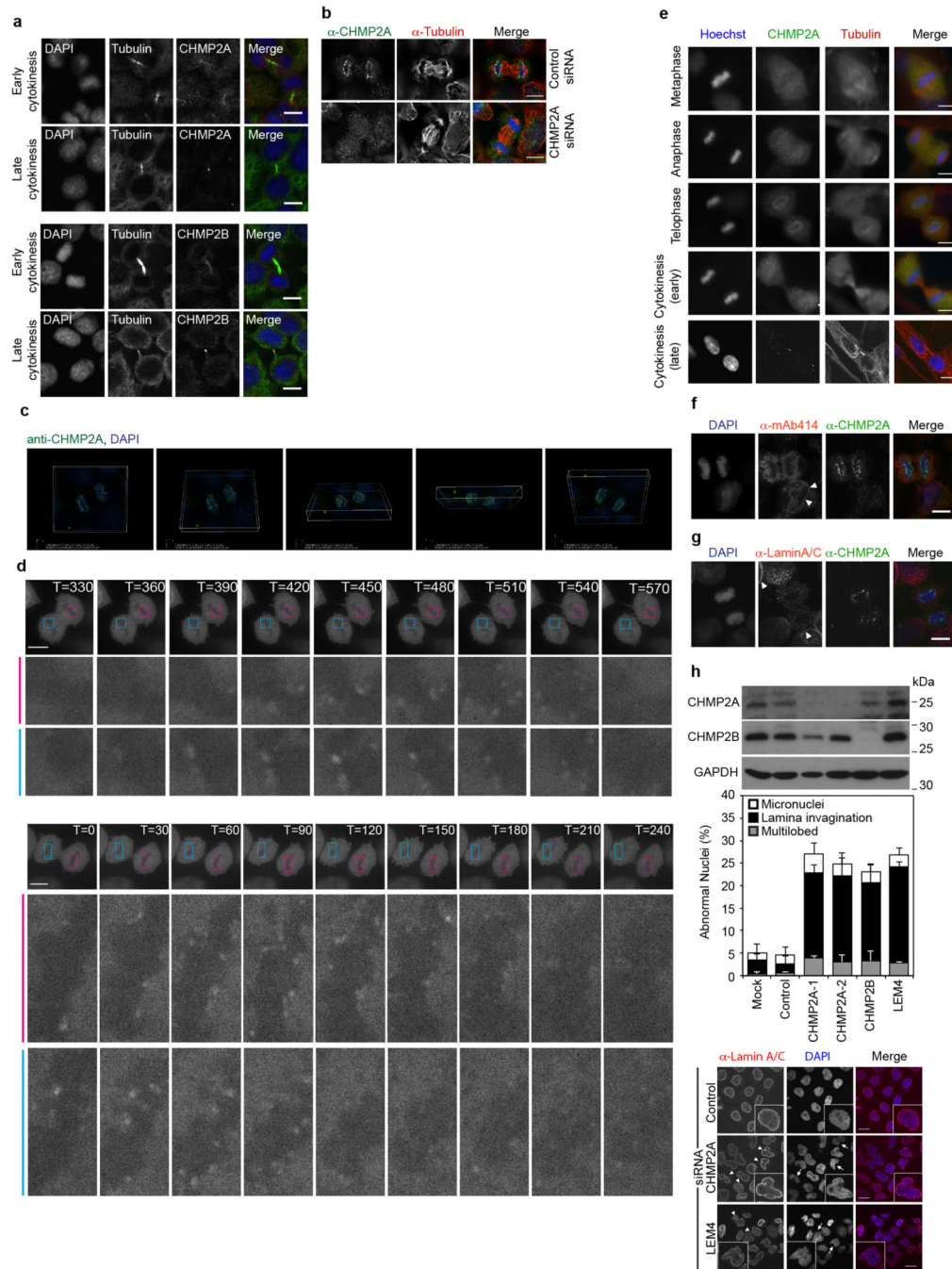
Requirements for CHMP2A localisation to the telophase NE were revealed through depletion of partner ESCRT-proteins, with CHMP4B and CHMP3, as for other ESCRT-dependent membrane remodeling events, playing a major role in this recruitment (Figure 2A). We employed siRNA-resistant FLAG-tagged CHMP2A expressed at near-endogenous levels to report localisation in the presence of CHMP2A siRNA (Figure 2B and 2C). Through introduction of mutations targeting known binding-partners, we found, as for midbody recruitment and cytokinetic abscission (Extended Data Figure 4A and 4B), and consistent with the previously determined telophase localisation of GFP-CHMP4B (Extended Data Figure 1D), that whilst CHMP2A<sup>R</sup>-FLAG localised to the forming NE, disrupting interaction with CHMP4 proteins by mutation of Arg24, Arg27 and Arg31 to Ala (CHMP2A<sup>R</sup>-FLAG RRR-AAA)<sup>16</sup> abolished this localisation. Mutation of the N-terminal CHMP2A  $\alpha_0$  helix<sup>19</sup>, or residues involved in the interaction with VPS4<sup>16</sup> had no effect on NE localisation (Figure 2C, Extended Data Figure 4A). These data indicate that CHMP2A is recruited to the forming NE through classical assembly of the ESCRT-III complex.

The p97 AAA-ATPase controls both phases of NE reformation; in concert with its adaptor protein p47, it regulates membrane delivery and NE expansion whilst through its adaptors Nuclear Protein Like 4 (NPL4) and UFD1 it regulates annular fusion<sup>6</sup>. Through NPL4 and UFD1, the p97 complex extracts ubiquitinated Aurora-B, a Chromosomal Passenger Complex (CPC) component, from chromatin to allow chromatin decondensation and membranation<sup>20,21</sup>. Given our observed ESCRT-III localisation (Figure 1) and known interactions of ESCRT-III components with the CPC<sup>13</sup>, we screened the ESCRT-machinery for interaction with the p97 complex by yeast 2-hybrid assay (Extended Data Figure 5A-D). We found that CHMP2A bound specifically to UFD1 and confirmed this interaction by direct-binding and co-precipitation assays (Figure 3A, 3B and Extended Data Figure 5E-H). We mapped the interaction with CHMP2A to the C-terminus of UFD1 (Extended Data Figure 5F and 5G) and found that truncation of the C-terminus of CHMP2A, or removal of the autoinhibitory helix ( $\alpha_5$ ), prevented interaction with UFD1 (Figure 3A). We employed siRNA targeting UFD1 (Extended Data Figure 6A); although its partner protein, p97, was required for EGFR degradation<sup>22</sup>, we found cells depleted for UFD1 degraded EGFR normally (Extended Data Figure 6B), allowed release of HIV-1 based lentivirus (Extended Data Figure 6C), and as previously reported<sup>21</sup>, completed cytokinesis normally (Extended Data Figure 6D). However, whilst cells depleted for UFD1 recruited CHMP2A to the midbody (Figure 3D), recruitment of CHMP2A to the forming NE was impaired (Figure 3C and 3D).

To examine mitotic roles for ESCRT-III in NE reformation, we imaged synchronised cultures of cells stably expressing Histone 2B-mCherry (H2B-mCh) and YFP-LAP2 $\beta$  and quantified the time taken to enclose the chromatin with YFP-LAP2 $\beta$  positive nuclear envelope. We were surprised to find that cells lacking ESCRT-III, but not UFD1, enclosed their chromatin faster than control cells (Extended Data Figure 7A-C). To explore the integrity of the nascent NE in CHMP2A depleted cells, we followed a protocol similar to that recently described<sup>23</sup> and imaged synchronised cultures of HeLa cells stably expressing both H2B-mCh and GFP-tagged  $\beta$ -Galactosidase ( $\beta$ -Gal) fused to the nuclear localisation signal (NLS) from Simian Virus 40 (GFP-NLS- $\beta$ Gal)<sup>24</sup>. GFP-NLS- $\beta$ Gal is released from the nucleus upon NE breakdown at mitotic onset and returned upon formation of transport-

competent nuclear pores during NE reformation (Extended Data Figure 8A and 8B). We found that the rate of GFP-NLS- $\beta$ Gal return to the nucleus was slower in ESCRT-III-depleted cells (Figure 4A-C), despite the cells having enclosed their chromatin with NE membranes faster (Extended Data Figure 7A). Whilst nuclei were frequently malformed in ESCRT-III-depleted cells (Extended Data Figure 1H<sup>17</sup>), incorporation of nuclear pore complexes and import machineries were normal (Extended Data Figure 8C-8E). However, in CHMP2A-, CHMP3- or UFD1-depleted cells, the post-mitotic nucleo-cytoplasmic partitioning of GFP-NLS- $\beta$ Gal was reduced (Figure 4B and 4C, Extended Data Figure 9A and 9B), indicating that NE integrity was compromised by treatments that prevent ESCRT-III assembly at the NE. Results were confirmed with a second reporter (GFP-NLS) (Extended Data Figure 9C) and we demonstrated that nuclear retention of this probe was defective in post-mitotic ESCRT-III depleted cells (Extended Data Figure 9D and 9E). Using correlative live-cell electron tomography, we found that CHMP2A depletion resulted in the persistence of unsealed holes in the post-mitotic NE (Figure 4D and 4E and Extended Data Figure 10A and 10B). Paralleling CHMP2 requirements in lentiviral release and cytokinetic abscission (Extended Data Figure 6C, and Extended Data Figure 9F), depletion of CHMP2B had minimal effect upon NE integrity (Extended Data Figure 9A and 9B), whilst co-depletion of CHMP2A and CHMP2B disrupted NE integrity to a greater extent than CHMP2A depletion alone (Figure 4B). NE integrity could be rescued by stable expression of siRNA-resistant CHMP2A-FLAG (CHMP2A<sup>R</sup>-FLAG), but, as with CHMP2A requirements in cytokinesis (Extended Data Figure 4B) and HIV-1 release<sup>16</sup>, not by expression of CHMP2A<sup>R</sup>-FLAG RRR-AAA (Figure 4F and 4G). We describe a novel localisation and function of ESCRT-III in NE remodeling at sites of annular fusion, a process strikingly similar to classical ESCRT-III mediated membrane remodeling (Extended Data Figure 10C). Localisation is governed by classical ESCRT-III assembly mechanisms and also requires UFD1. An equivalent ESCRT-III-dependent membrane remodeling at the NE may allow viruses or megaRNPs to traverse this membrane<sup>25-27</sup> and in yeast, ESCRT-III has recently been shown to participate in surveillance and extraction of defective nucleoporins at the IMN<sup>28</sup> indicating additional ESCRT-III activities on this membrane may exist throughout the cell cycle. ESCRT-III is thus involved in regulating the quality of the NE and gene expansion within the ESCRT-machinery may have resulted from an evolutionary drive to accommodate open mitoses.

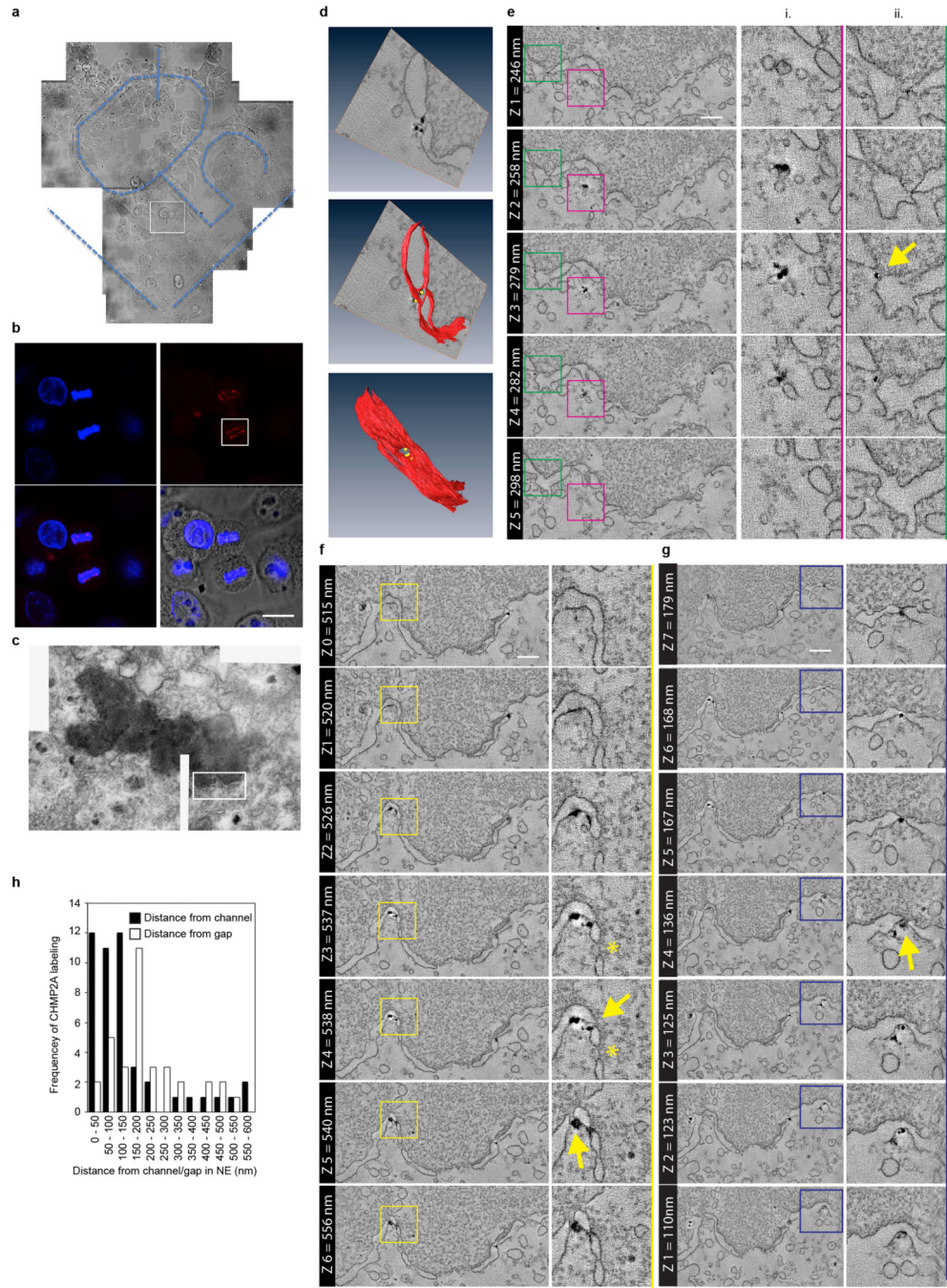
Extended Data



**Extended Data Figure 1. Localisation of ESCRT components during the cell cycle**

A, B. Immunofluorescence analysis of HeLa cells stained with anti-tubulin, anti-CHMP2A or -CHMP2B and DAPI (A). Images in A representative of 2 acquired images per field of view. Cells in B were treated with Control or CHMP2A-targeting siRNA, images representative of 4 acquired images (control) or 2 acquired images (CHMP2A siRNA). C. Deconvolved projections of HeLa cells stained with anti-CHMP2A and DAPI, corresponds

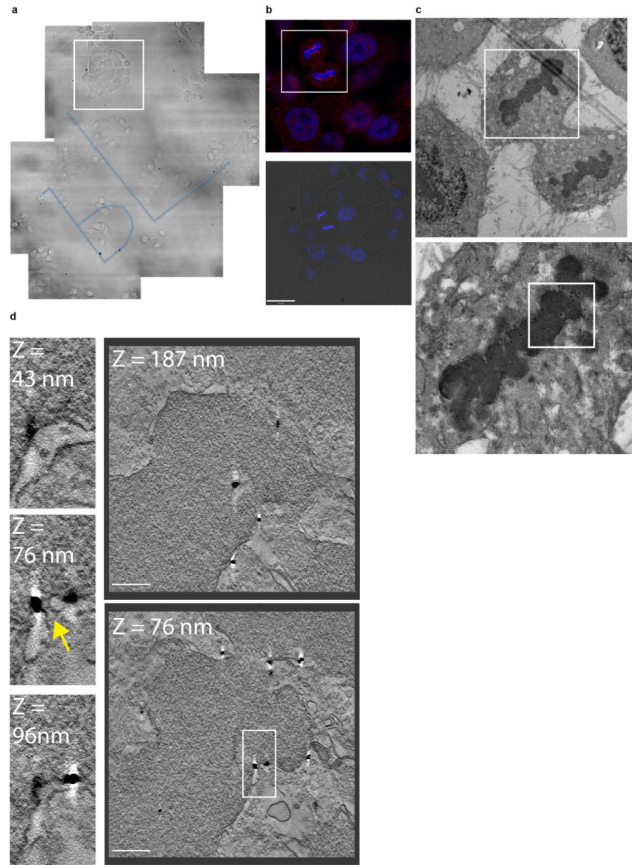
to stills from Supplemental Video 1, images representative of 2 deconvolved image series. D. HeLa cells stably expressing GFP-CHMP4B were imaged live during the anaphase to telophase transition. Telophase frames at 30 second intervals are presented, corresponding to stills from Supplemental Video 2, images representative of 4 acquisitions. E. Immunofluorescence analysis of human diploid fibroblasts stained with anti-CHMP2A, anti-tubulin and DAPI, images representative of 3 acquired cells per cell cycle phase. F, G. Immunofluorescence analysis of HeLa cells stained with anti-CHMP2A, DAPI and either, anti-mAb414 (F) or anti-LaminaA/C (G), images representative of 5 acquired cells. Arrowheads indicate regions of formed nuclear pores or lamina as indicated. H. Quantification of abnormal nuclei (the presence of multiple lobes, micronuclei, lamina ingression or invagination) in HeLa cells transfected with the indicated siRNA and stained with anti-LaminaA/C (1300 cells over 5 experiments quantified per treatment  $\pm$  S.D.). Images representative of 3 (control, CHMP2A siRNA) or 2 (LEM4 siRNA) acquired fields of view and resolved cell lysates were examined by western blotting with anti-CHMP2A, anti-CHMP2B or anti-GAPDH antisera as indicated. In all cases, scale bar is 10  $\mu$ m.



**Extended Data Figure 2. Correlative light and electron microscopy of endogenous CHMP2A localisation in telophase NE**

A-C. Phase contrast (A), correlative immunofluorescence (B, scale bar is 10  $\mu$ m) and transmission electron microscopy of HeLa cells stained with anti-CHMP2A, detected by Alexa<sup>594</sup>-fluorogold and DAPI. Boxed region in A is shown in B, boxed region in B is shown in C, in all cases, images representative of 3 cells prepared for CLEM. D. 3D rendering of tomographic reconstruction of forming NE from boxed region in C and Figure 1D, a single example of a nucleocytoplasmic channel was selected for 3D rendering. E-G. Z-slices extracted from tomographic reconstructions of forming NE depicting CHMP2A-

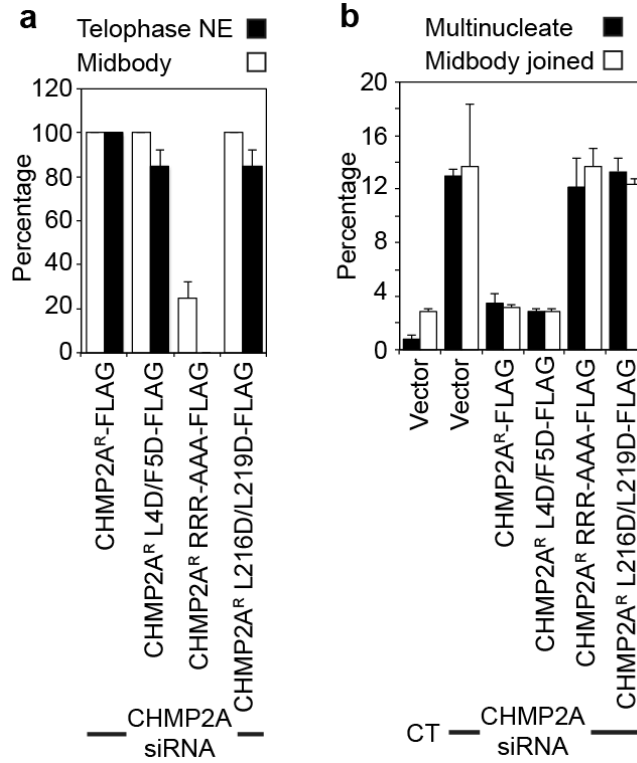
localisation to isolated vesicles (Ei) and nucleo-cytoplasmic channels (arrows in Eii, F, G) at the indicated Z-heights, scale bar is 200 nm. Localisation of CHMP2A to nucleocytoplasmic channels was observed in 3 independent cells, data from a second cell are presented in Extended Data Figure 3. Note CHMP2A localisation to nucleocytoplasmic channels is distinct from nuclear pores (asterisk in Extended Data Figure 2F). H. Quantification of CHMP2A labeling from 2 independently prepared cells, channels were defined as discontinuities up to 80 nm, and gaps were defined as discontinuities over 80 nm. Distances of the gold-particles from channels or gaps were measured on the tomograms in 3-dimensions and plotted as a histogram. The majority (74.4%) of gold label was found within 150 nm of nucleo-cytoplasmic channels and the majority (70.6 %) of the gold label was found more than 150 nm from the larger gaps in the NE.



**Extended Data Figure 3. Correlative light and electron microscopy of endogenous CHMP2A localisation in telophase NE**

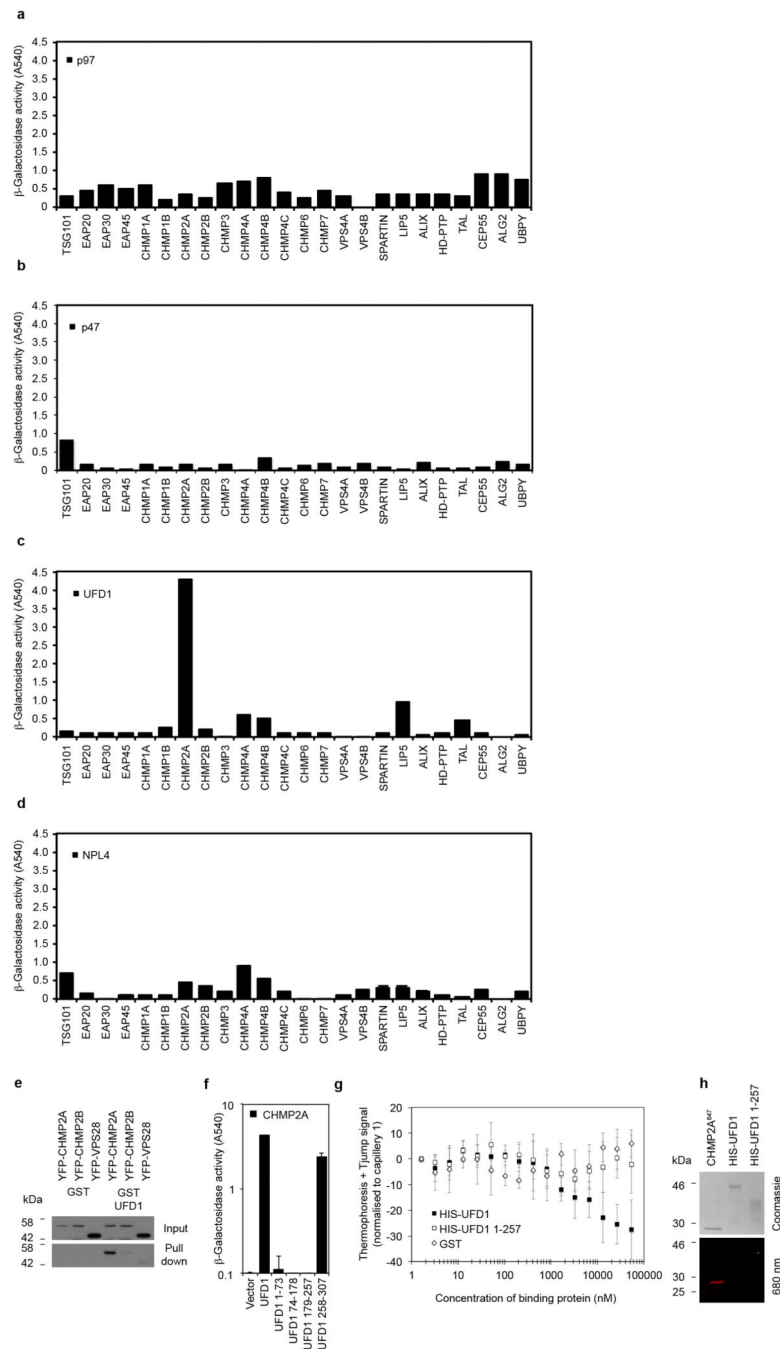
A-C. Phase contrast (A), correlative immunofluorescence (B) and transmission electron microscopy (C) of a second HeLa cell stained with anti-CHMP2A, detected by Alexa<sup>594</sup>-fluoronanogold and DAPI. Boxed region in A is shown in B, boxed region in B is shown in C. D. Z-slices extracted from tomographic reconstruction of forming NE from boxed region in C depicting CHMP2A-localisation to nucleo-cytoplasmic channels at the indicated Z-heights. Arrow indicates nucleocytoplasmic channel, scale bar is 200 nm, images in all cases

representative of 3 cells processed for CLEM, quantification of gold localisation given in Extended Data Figure 2H.



**Extended Data Figure 4. Mitotic defects in cells reliant on mutated forms of CHMP2A**

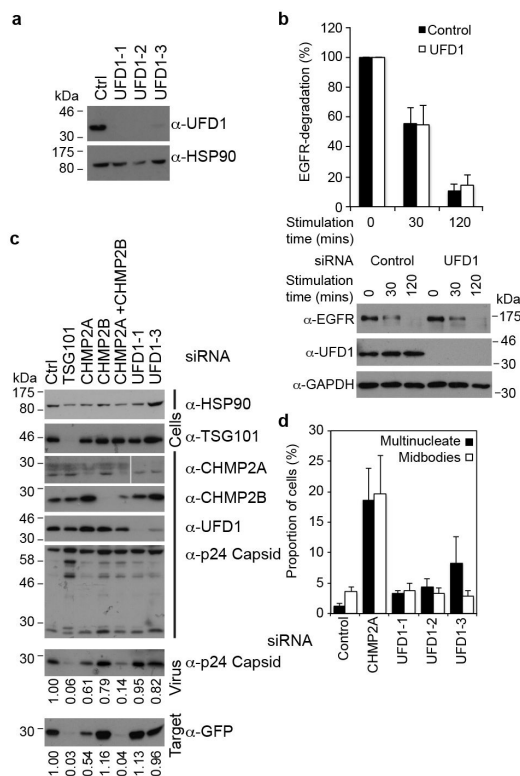
A. Quantification of CHMP2A recruitment to the telophase NE or the midbody from Figure 2C (n = 3 ± S.D., 10 cells (midbody or telophase) scored per experiment). B. Quantification of cytokinetic failure from cells treated with the indicated siRNA (300 cells were quantified per experiment, from 3 independent experiments ± S.D.).



### Extended Data Figure 5. Screening for ESCRT : p97 complex interactions

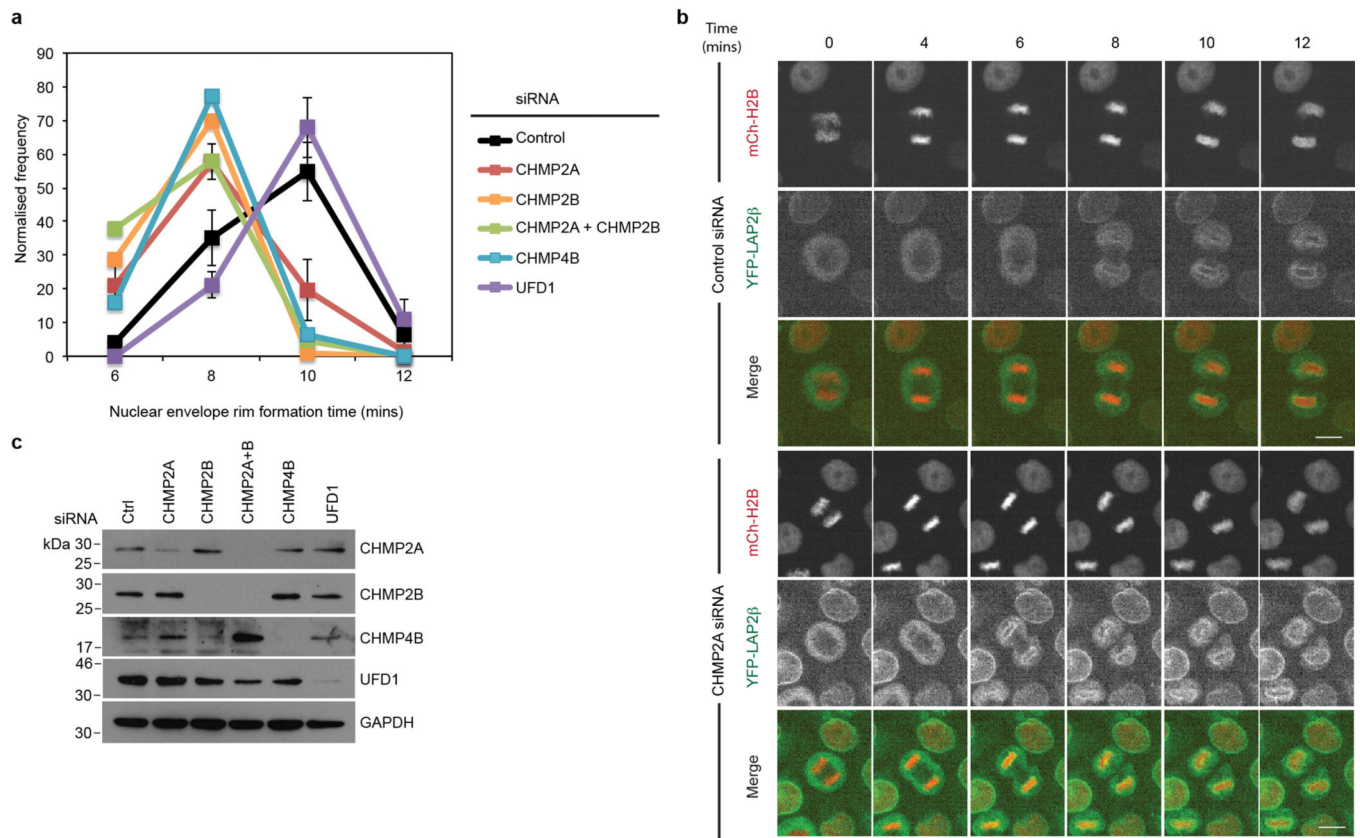
A-D. β-galactosidase activity of yeast co-transformed with the indicated Gal4 (ESCRT) and VP16 fused proteins (n = 2). E. Resolved cell lysates and glutathione-bound fractions from 293T cells transfected with the indicated fusion proteins were examined by western blotting with anti-GFP (n = 3). F. β-galactosidase activity of yeast co-transformed with the indicated Gal4 and VP16 fused proteins (n = 3 ± S.D.). G. MST experiments detailing binding of CHMP2A to GST (n = 4), HIS-UFD1 (n = 5) or HIS-UFD1 1-257 (n = 4, ± S.D.). As no reduction in thermophoresis signal was observed for GST or His-UFD1 1-257 across the

concentration range, we present here the average thermophoresis signal change at equivalent protein concentrations for these three proteins, normalized to zero at the concentration in capillary 1. H. CHMP2A<sup>647</sup>, HIS-UFD1 and HIS-UFD1 1-257 were examined by IR imaging or coomassie staining.



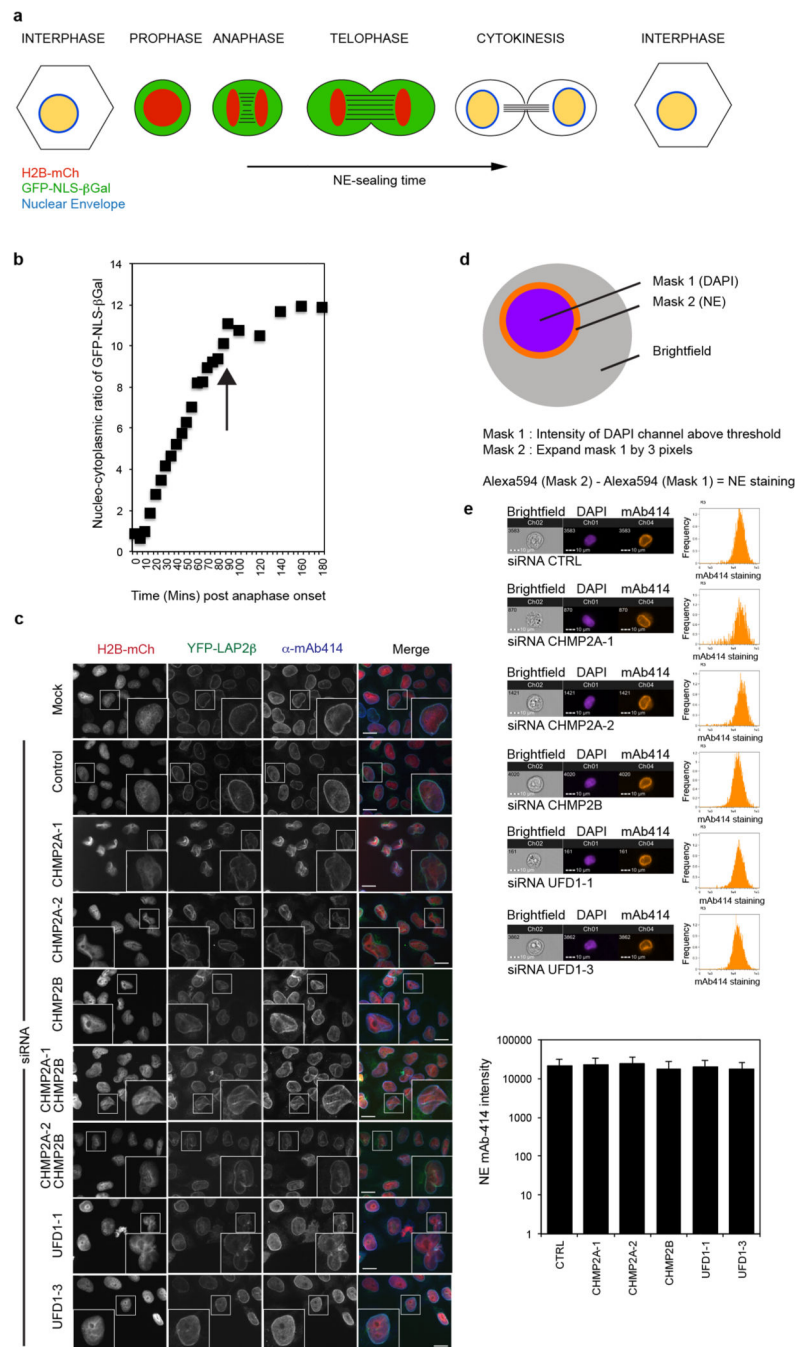
#### Extended Data Figure 6. UFD1 depletion does not effect ESCRT-dependent receptor degradation, lentivirus release or cytokinetic abscission

A. Resolved cell lysates of HeLa cells transfected with the indicated siRNA were examined by western blotting with anti-UFD1 or anti-HSP90 antisera. B. Resolved lysates of human diploid fibroblasts transfected with the indicated siRNA and treated for the indicated times with epidermal growth factor (20 ng/ml) were examined by western blotting with anti-EGFR, anti-UFD1 and anti-GAPDH antisera. EGFR degradation was quantified by densitometry ( $n = 3$ ,  $\pm$  S.D.). C. Resolved cell lysates from 293T cells transfected with the indicated HIV-1 based lentiviral plasmids, a virally packaged GFP-plasmid, and the indicated siRNA were examined by western blotting with anti-p24 capsid, -HSP90, -TSG101, -CHMP2A, -CHMP2B and -UFD1 antibodies. Viral supernatants were collected and used to infect target HeLa cells. Resolved virions present in the 293T supernatant were examined by western blotting with anti-p24 capsid. Resolved lysates of infected HeLa cells were examined by western blotting with anti-GFP. Virion release was the ratio of released to cellular p24-capsid, as quantified by densitometry ( $n = 2$ ); infectivity was quantified as GFP-signal in target cells, as quantified by densitometry ( $n = 2$ ). D. siRNA-transfected HeLa cells were fixed and stained with anti-Tubulin. Multinucleate cells ( $n = 5$ ,  $\pm$  S.D.) or cells connected by midbodies ( $n = 5$ ,  $\pm$  S.D.) were scored visually, 300 cells scored per experiment.



### Extended Data Figure 7. ESCRT-depletion impairs NE-rim formation

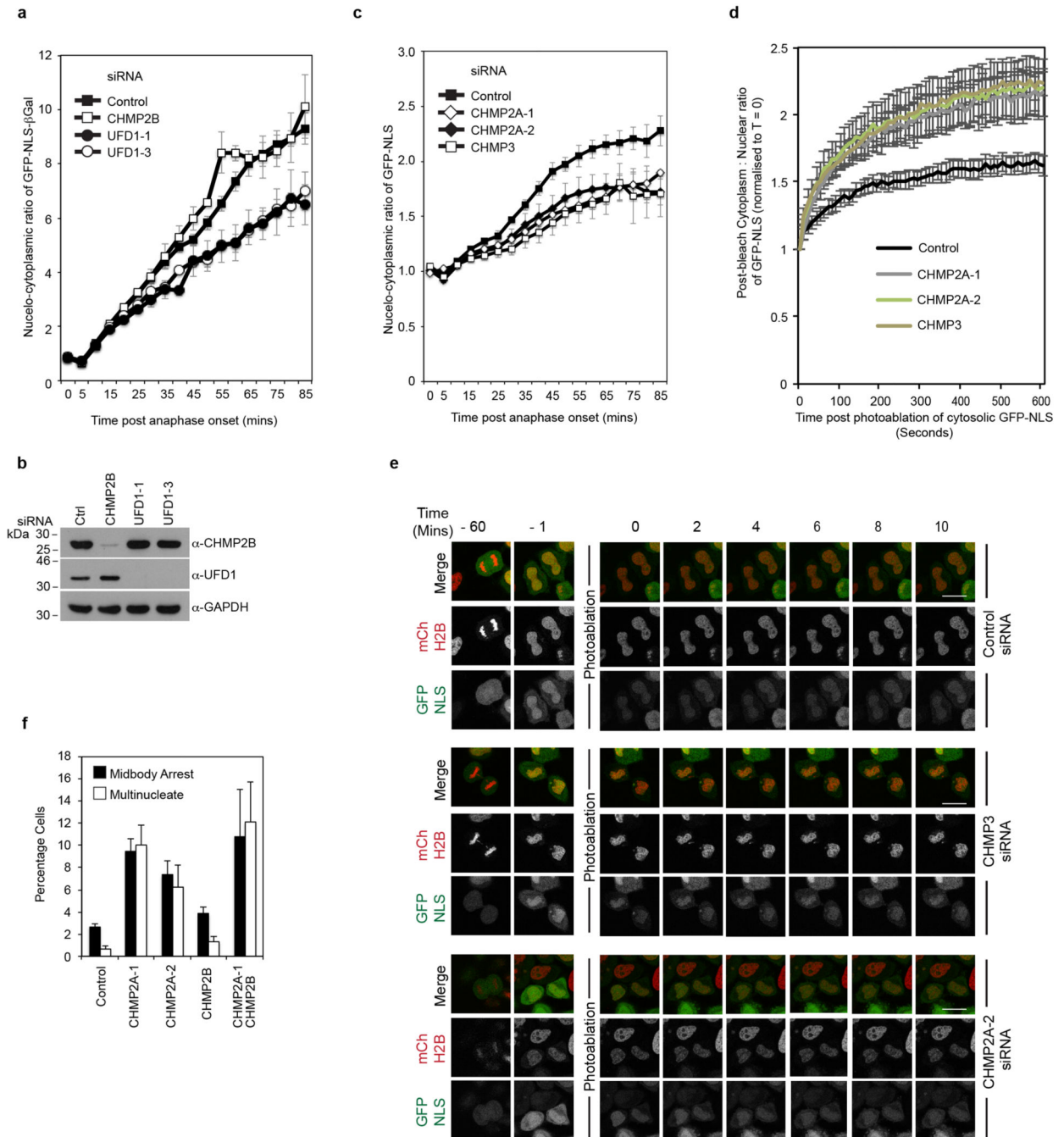
A,B. Timelapse microscopy analysis and quantification of NE-rim formation in HeLa cells stably expressing YFP-LAP2 $\beta$  and mCh-H2B and treated with the indicated siRNA Scale bar is 10  $\mu$ m. Time for rim formation post anaphase onset given (mins) (Ctrl  $8.53 \pm 0.09$ , 226 cells analysed over 8 independent experiments; CHMP2A-1,  $7.60 \pm 0.09$ , 205 cells analysed over 7 independent experiments; CHMP2A-2,  $6.86 \pm 0.12$ , 37 cells analysed over 2 independent experiments; CHMP2B,  $6.92 \pm 0.09$ , 79 cells analysed over 4 independent experiments; CHMP2A and CHMP2B,  $6.84 \pm 0.13$ , 50 cells analysed over 2 independent experiments; CHMP4B,  $7.07 \pm 0.14$ , 44 cells analysed over 2 independent experiments; UFD1  $9.2 \pm 0.18$ , 39 cells analysed over 3 independent experiments. All times mean  $\pm$  S.E.M, in minutes, images representative of the indicated number of cell analysed). C. Resolved cell lysates from A were analysed by western-blotting with the indicated antisera.



### Extended Data Figure 8. ESCRT-depletion does not impair nuclear pore formation

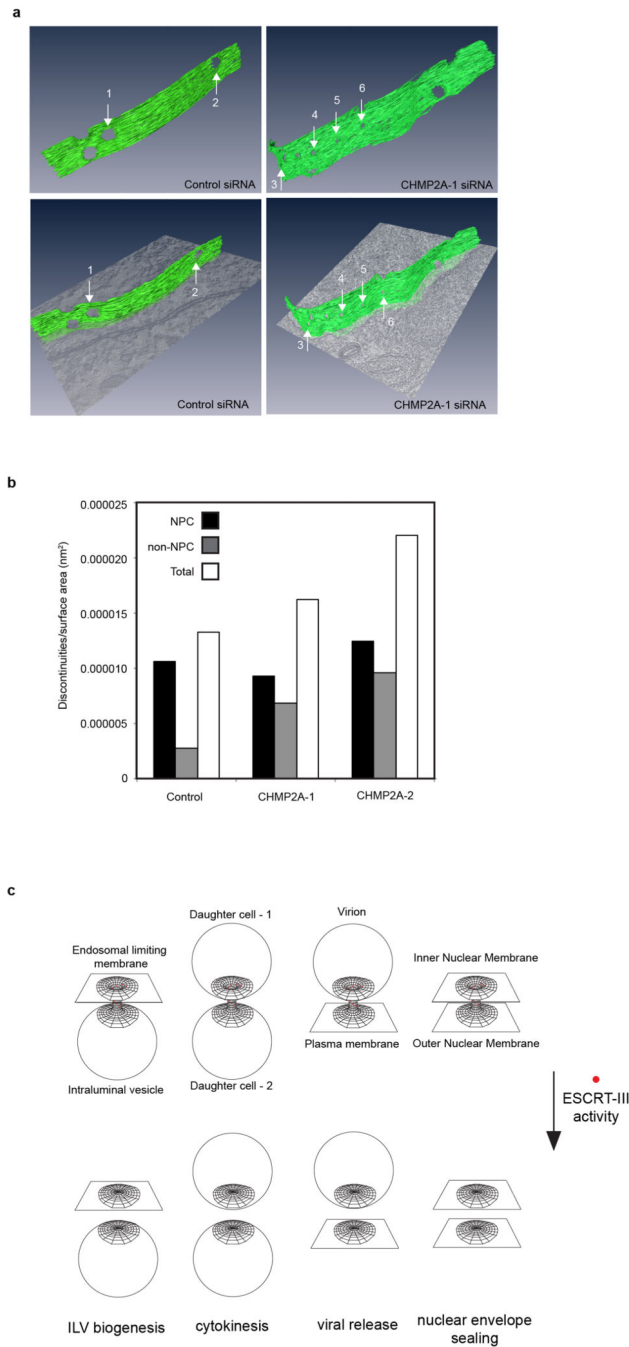
A. Schematic of nuclear envelope integrity assay. B. Control siRNA treated HeLa cells reporting nucleo-cytoplasmic partitioning using the GFP-NLS-βGal assay, average NE compartmentalisation from 20 cells presented. Nucleo-cytoplasmic partitioning stabilises at 85 minutes (indicated by arrow). C. Immunofluorescence analysis of HeLa cells stably expressing YFP-LAP2β transfected with the indicated siRNA then stained with anti-mAb414 and DAPI (n = 3), Scale bar is 10 μm. D. Mask employed to quantify nuclear pore formation by image-based flowcytometry (Imagestream). E. Imagestream analysis of HeLa

cells transfected with the indicated siRNA, then stained with anti-mAb414 and DAPI. Nuclear pore intensity quantified by mask described in D. Representative images from 2 independent experiments, histogram and population averages displayed, graphical quantification of NPC intensity from the indicated number of gated cells (Control, 3045; CHMP2A-1, 1256; CHMP2A-2, 2152; CHMP2B, 5237; UFD1-1, 4146; UFD1-3, 4325; error bars are  $\pm$  S.D.).



Extended Data Figure 9. Requirements for nucleocytoplasmic compartmentalization

A. Quantification of NE-sealing from siRNA treated cells as in Figure 4B, (Ctrl 140 cells from 7 independent experiments; UFD1-1, 60 cells from 3 independent experiments,  $P = 0.044$ ; UFD1-3, 60 cells from 3 independent experiments,  $P = 0.021$ ; CHMP2B 40 cells from 2 independent experiments, N.S. All times quoted  $\pm$  S.E.M. in minutes; 2-tailed student's T-test was used to assess significance at the 85-minute timepoint). B. Resolved cell lysates from A were analysed by western-blotting with the indicated antisera. C. Nuclear envelope integrity assay as performed with cells stably expressing mCh-H2B and GFP-NLS and transfected with the indicated siRNA. Differences in nucleocytoplasmic partitioning was assessed after plateau at the 65 minute timepoint using a 2-tailed Student's T-test : (Ctrl, 79 cells from 4 independent experiments, CHMP2A-1, 60 cells from 3 independent experiments,  $P = 0.048$ ; CHMP2A-2, 52 cells from 3 independent experiments,  $P = 0.011$ ; CHMP3, 28 cells from 3 independent experiments,  $P = 0.028$ , error bars represent S.E.M.). D, E. HeLa cells stably expressing mCh-H2B and GFP-NLS were transfected with the indicated siRNA and imaged live. 60 minutes post anaphase onset, cytoplasmic signal was photo-ablated ( $T = 0$ ) and Recovery of cytoplasmic signal from the nuclear pool was calculated for the indicated conditions (Cytoplasmic : Nuclear ratio of GFP-NLS was normalized to  $T = 0$ . Ctrl, 21 cells from 4 independent experiments; CHMP2A-1, 24 cells from 4 independent experiments,  $P = 0.04$ ; CHMP2A-2, 23 cells from 4 independent experiments,  $P = 0.05$ ; CHMP3, 15 cells from 3 independent experiments,  $P = 0.004$ , 2-tailed Student's t-test was used to assess significance after 10 minutes. In D, error bars represent S.E.M. in E, scale bar is 10  $\mu\text{m}$ . F. Scoring of multinucleate and midbody-connected HeLa cells transfected with the indicated siRNA and stained with anti-tubulin and DAPI (300 cells analysed per condition,  $n = 4 \pm$  S.D.).



**Extended Data Figure 10. Affect of CHMP2A depletion on NE discontinuities**

A. Presentation of reconstructed tomograms from Figure 4D. B. CHMP2A-depleted cells exhibited more non-NPC discontinuities per unit area whilst the number of NPC per unit area was constant, tomograms as described in Figure 4E were scored for discontinuities. The internal diameter of NPCs was slightly reduced in CHMP2A-depleted cells (Control  $84 \pm 7.6$  nm, CHMP2A-1,  $74 \pm 8.8$  nm; CHMP2A-2,  $74 \pm 5.7$  nm). C. Schematic depicting topological equivalent of ESCRT-III-dependent membrane fusion events.

## Supplementary Material

Refer to Web version on PubMed Central for supplementary material.

## Acknowledgements

JCG is a Wellcome Trust Research Career Development Fellow. We acknowledge the Nikon Imaging Centre at KCL and the NIHR Comprehensive Biomedical Research Centre at Guy's and St Thomas' NHS Foundation Trust for access to core equipment. We thank the staff of the Wolfson Bioimaging Facility for their support. We thank Prof Juan Martin-Serrano (KCL) for gifts of plasmids and cells.

## References

1. Burke B. The nuclear envelope: filling in gaps. *Nat. Cell Biol.* 2001; 3:E273–4. [PubMed: 11781582]
2. Anderson DJ, Hetzer MW. Shaping the endoplasmic reticulum into the nuclear envelope. *J. Cell. Sci.* 2008; 121:137–142. [PubMed: 18187447]
3. Schooley A, Vollmer B, Antonin W. Building a nuclear envelope at the end of mitosis: coordinating membrane reorganization, nuclear pore complex assembly, and chromatin decondensation. *Chromosoma.* 2012; 121:539–554. [PubMed: 23104094]
4. Burke B, Ellenberg J. Remodelling the walls of the nucleus. *Nat. Rev. Mol. Cell Biol.* 2002; 3:487–497. [PubMed: 12094215]
5. Lu L, Ladinsky MS, Kirchhausen T. Formation of the postmitotic nuclear envelope from extended ER cisternae precedes nuclear pore assembly. *J. Cell Biol.* 2011; 194:425–440. [PubMed: 21825076]
6. Hetzer M, et al. Distinct AAA-ATPase p97 complexes function in discrete steps of nuclear assembly. *Nat. Cell Biol.* 2001; 3:1086–1091. [PubMed: 11781570]
7. McCullough J, Colf LA, Sundquist WI. Membrane Fission Reactions of the Mammalian ESCRT Pathway. *Annu. Rev. Biochem.* 2013 doi:10.1146/annurev-biochem-072909-101058.
8. Carlton JG, Agromayor M, Martin-Serrano J. Differential requirements for Alix and ESCRT-III in cytokinesis and HIV-1 release. *Proc. Natl. Acad. Sci. U.S.A.* 2008; 105:10541–10546. [PubMed: 18641129]
9. Carlton JG, Martin-Serrano J. Parallels between cytokinesis and retroviral budding: a role for the ESCRT machinery. *Science.* 2007; 316:1908–1912. [PubMed: 17556548]
10. Elia N, Sougrat R, Spurlin TA, Hurley JH, Lippincott-Schwartz J. Dynamics of endosomal sorting complex required for transport (ESCRT) machinery during cytokinesis and its role in abscission. *Proc. Natl. Acad. Sci. U.S.A.* 2011; 108:4846–4851. [PubMed: 21383202]
11. Morita E, et al. Human ESCRT and ALIX proteins interact with proteins of the midbody and function in cytokinesis. *EMBO J.* 2007; 26:4215–4227. [PubMed: 17853893]
12. Jouvenet N, Zhadina M, Bieniasz PD, Simon SM. Dynamics of ESCRT protein recruitment during retroviral assembly. *Nat. Cell Biol.* 2011; 13:394–401. [PubMed: 21394083]
13. Carlton JG, Caballe A, Agromayor M, Kloc M, Martin-Serrano J. ESCRT-III governs the Aurora B-mediated abscission checkpoint through CHMP4C. *Science.* 2012; 336:220–225. [PubMed: 22422861]
14. Clever M, Funakoshi T, Mimura Y, Takagi M, Imamoto N. The nucleoporin ELYS/Mel28 regulates nuclear envelope subdomain formation in HeLa cells. *Nucleus.* 2012; 3:187–199. [PubMed: 22555603]
15. Stauffer DR, Howard TL, Nyun T, Hollenberg SM. CHMP1 is a novel nuclear matrix protein affecting chromatin structure and cell-cycle progression. *J. Cell. Sci.* 2001; 114:2383–2393. [PubMed: 11559747]
16. Morita E, et al. ESCRT-III protein requirements for HIV-1 budding. *Cell Host Microbe.* 2011; 9:235–242. [PubMed: 21396898]
17. Morita E, et al. Human ESCRT-III and VPS4 proteins are required for centrosome and spindle maintenance. *Proc. Natl. Acad. Sci. U.S.A.* 2010; 107:12889–12894. [PubMed: 20616062]

18. Asencio C, et al. Coordination of kinase and phosphatase activities by Lem4 enables nuclear envelope reassembly during mitosis. *Cell*. 2012; 150:122–135. [PubMed: 22770216]
19. Buchkovich NJ, Henne WM, Tang S, Emr SD. Essential N-terminal insertion motif anchors the ESCRT-III filament during MVB vesicle formation. *Dev. Cell*. 2013; 27:201–214. [PubMed: 24139821]
20. Ramadan K, et al. Cdc48/p97 promotes reformation of the nucleus by extracting the kinase Aurora B from chromatin. *Nature*. 2007; 450:1258–1262. [PubMed: 18097415]
21. Dobrynin G, et al. Cdc48/p97-Ufd1-Npl4 antagonizes Aurora B during chromosome segregation in HeLa cells. *J. Cell. Sci.* 2011; 124:1571–1580. [PubMed: 21486945]
22. Ritz D, et al. Endolysosomal sorting of ubiquitylated caveolin-1 is regulated by VCP and UBXD1 and impaired by VCP disease mutations. *Nat. Cell Biol.* 2011; 13:1116–1123. [PubMed: 21822278]
23. Anderson DJ, Hetzer MW. Reshaping of the endoplasmic reticulum limits the rate for nuclear envelope formation. *J. Cell Biol.* 2008; 182:911–924. [PubMed: 18779370]
24. Sorg G, Stamminger T. Mapping of nuclear localization signals by simultaneous fusion to green fluorescent protein and to beta-galactosidase. *BioTechniques*. 1999; 26:858–862. [PubMed: 10337476]
25. Lee C-P, et al. The ESCRT machinery is recruited by the viral BFRF1 protein to the nucleus-associated membrane for the maturation of Epstein-Barr Virus. *PLoS Pathog.* 2012; 8:e1002904. [PubMed: 22969426]
26. Pawliczek T, Crump CM. Herpes simplex virus type 1 production requires a functional ESCRT III complex but is independent of TSG101 and ALIX expression. *J. Virol.* 2009; 83:11254–11264. [PubMed: 19692479]
27. Speese SD, et al. Nuclear envelope budding enables large ribonucleoprotein particle export during synaptic Wnt signaling. *Cell*. 2012; 149:832–846. [PubMed: 22579286]
28. Webster BM, Colombi P, Jäger J, Lusk CP. Surveillance of Nuclear Pore Complex Assembly by ESCRT-III/Vps4. *Cell*. 2014; 159:388–401. [PubMed: 25303532]

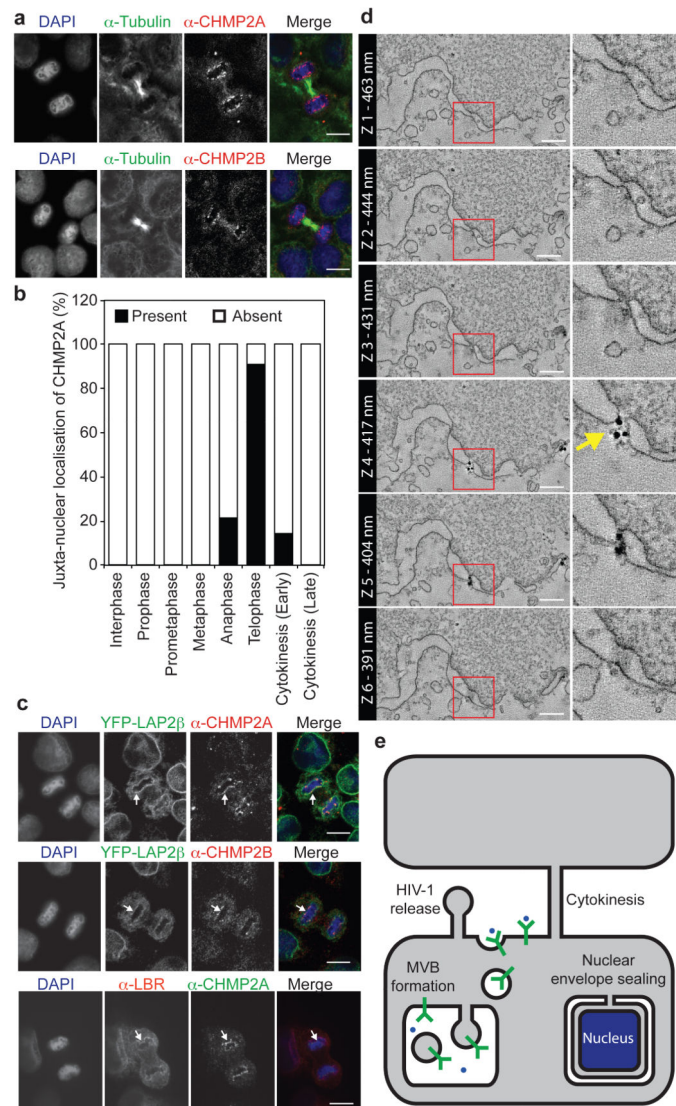


### Figure 1. ESCRT-III localises to the forming nuclear envelope

A. HeLa cells stained with anti-tubulin, either anti-CHMP2A or anti-CHMP2B and 4',6-diamidino-2-phenylindole (DAPI). Scale bar is 10  $\mu$ m, images representative of 3 acquired images in each case. B. Quantification of juxta-nuclear CHMP2A localisation during mitosis from A, quantification from 20 cells in interphase, prophase, pro-metaphase and metaphase, 23 cells in anaphase, 24 cells in telophase, 36 cells in early cytokinesis and 20 cells in late cytokinesis. C. HeLa cells stained with DAPI, anti-CHMP2A or anti-CHMP2B and either stably expressing YFP-LAP2 $\beta$ , or stained with anti-LBR. Arrows indicate regions of colocalisation. Scale bar is 10  $\mu$ m, images representative of 2 (anti-CHMP2B and YFP-LAP2 $\beta$ , anti-LBR and anti-CHMP2A) or 4 (anti-CHMP2A and YFP-LAP2 $\beta$ ) acquired images. D. Tomographic slices of HeLa cells stained with fluoronanogold anti-CHMP2A. Correlation depicted in Extended Data Figure 2A-2C, arrow indicates nucleocytoplasmic channel, scale bar is 200 nm, image representative of 25 gold-decorated nucleocytoplasmic channels and quantified in Extended Data Figure 2H. E. Schematic depicting topological

equivalence between annular fusion of the NE and ESCRT-dependent membrane fusion events.

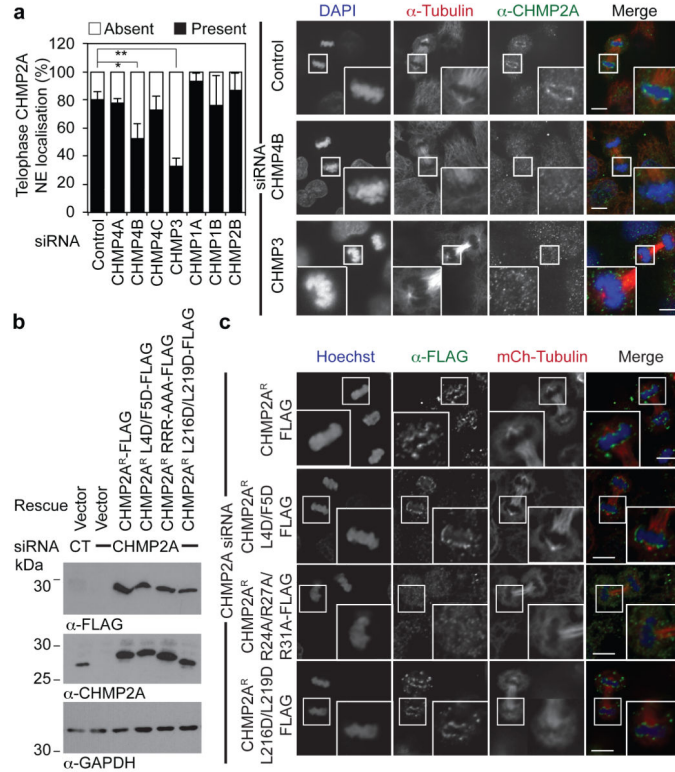


**Figure 2. Classical ESCRT-interactions govern CHMP2A telophase-NE localisation**

A. Immunofluorescence and quantification of NE localisation in HeLa cells transfected with the indicated siRNA and stained with anti-CHMP2A, anti-tubulin and DAPI (Number of cells scored from 4 independent experiments: Control, 58; CHMP4A, 59; CHMP4B, 55; CHMP4C, 53; CHMP3, 64; CHMP1A, 47; CHMP1B 52; CHMP2B, 44. Percentage NE localisation given  $\pm$  S.D. \*  $P = 0.014$ , \*\*  $P = 0.0004$  (2-tailed Student's T-test), Scale bar is 10  $\mu\text{m}$ , images representative of 47 cells (Control), 26 cells (CHMP4B siRNA) and 42 cells (CHMP3 siRNA). B. Western blotting of lysates from siRNA-depleted HeLa cells stably expressing mCherry-tubulin and the indicated CHMP2A<sup>R</sup>-FLAG with anti-FLAG, anti-CHMP2A or anti-GAPDH antisera. C. Immunofluorescence of CHMP2A<sup>R</sup>-FLAG recruitment to the telophase NE in CHMP2A-depleted cells. Scale bar is 10  $\mu\text{m}$ , quantification in Extended Data Figure 4A, images representative of 30 cells (Control), 26 cells (L4D/F5D), 30 cells (RRR-AAA) and 26 cells (L216D/L219D).

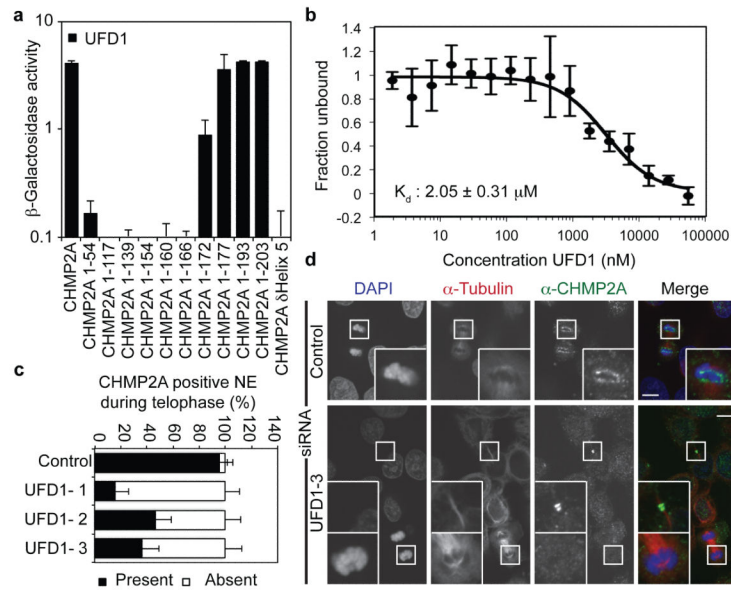


### Figure 3. UFD1 directs NE-localisation of CHMP2A

A.  $\beta$ -galactosidase activity of yeast co-transformed with the indicated Gal4 and VP16 fused proteins ( $n = 3 \pm \text{S.D.}$ ). B. MST experiments displaying interaction of HIS-UFD1 with CHMP2A (Fraction unbound displayed,  $n = 5 \pm \text{S.D.}$ ) C, D. Immunofluorescence (D) and quantification of NE localisation (C: Control, 35 cells; UFD1-1, 42 cells; UFD1-2, 25 cells; UFD1-3, 39 cells; average  $\pm \text{S.D.}$  presented from 4 independent experiments) in HeLa cells transfected with the indicated siRNA and stained with anti-CHMP2A, anti-tubulin and DAPI, scale bar is 10  $\mu\text{m}$ , images representative of 23 cells (Control), 34 cells (UFD1-1) 14 cells (UFD1-2) and 24 cells (UFD1-3).

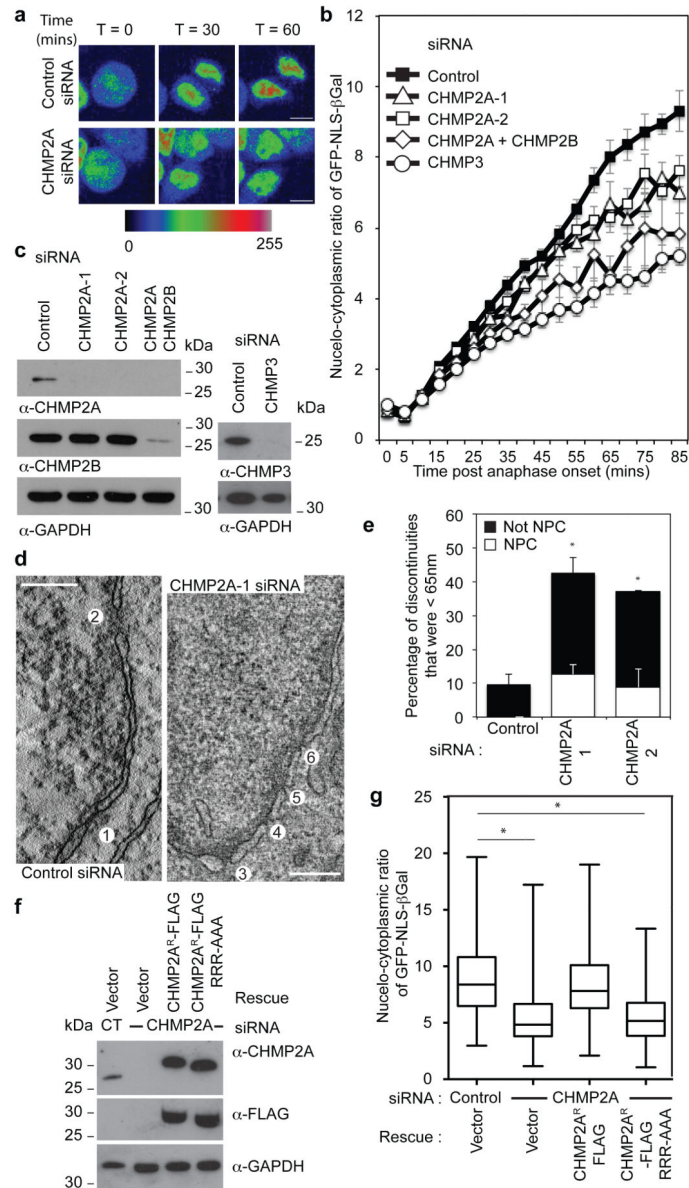


#### Figure 4. ESCRT-III depletion disrupts nuclear envelope integrity

A. Timelapse analysis of NE-sealing in siRNA transfected HeLa cells stably expressing H2B-mCh and GFP-NLS-βGal. GFP-signal presented according to pseudocolour scale at the indicated timepoints. Scale bar is 10 μm, a single image was pseudocoloured for demonstrative purposes. B. Quantification of NE-sealing from siRNA treated cells as in A, (Cells were quantified at each time point; Ctrl 140 cells from 7 independent experiments; CHMP2A-1, 98 cells from 5 independent experiments,  $P = 0.047$ ; CHMP2A-2, 80 cells from 4 independent experiments,  $P = 0.023$ ; CHMP2A + CHMP2B, 60 cells from 3 independent experiments,  $P = 0.006$ ; CHMP3, 34 cells from 3 independent experiments,  $P = 0.002$ . All values quoted  $\pm$  S.E.M.; 2-tailed Student's t-test used to assess significance after 85 minutes). C. Western blotting of cell lysates from B with anti-CHMP2A, anti-CHMP2B anti-CHMP3 or anti-GAPDH antisera. D. Z-slices extracted from a correlative tomographic

reconstruction of the NE at 60 minutes post anaphase onset from the indicated siRNA-transfected mCh-Tub HeLa cells. The numbered circles correspond to discontinuities labeled in the 3D reconstructions in Extended Data Figure 10A, scale bar is 200 nm, image representative of 6 (control) and 12 (CHMP2A-1 siRNA) tomographic reconstructions. E. The percentage of discontinuities smaller than 65 nm was scored. Discontinuities in this range that were not NPCs as a percentage of total discontinuities (including NPCs) for n number of reconstructed tomograms: Control  $9.4 \pm 3.0$ , n = 6; CHMP2A-1,  $29.9 \pm 4.7$ , P = 0.01, n = 12; CHMP2A-2,  $28.3 \pm 2.0$ , P = 0.021, n = 2. The increase in the percentage of non-NPC discontinuities was assessed by 2-tailed Student's T-test (average diameter of non-NPC discontinuities was  $38 \pm 22$  nm (CHMP2A-1) and  $58 \pm 19$  nm (CHMP2A-2)). F. Western blotting of lysates from siRNA-treated HeLa cells stably expressing H2B-mCh, GFP-NLS- $\beta$ Gal and siRNA-resistant CHMP2A<sup>R</sup>-FLAG with anti-CHMP2A, anti-FLAG or anti-GAPDH antisera. G. Quantification of NE-sealing from cells treated with siRNA as in F and imaged from 4 independent experiments, (Mean nucleo-cytoplasmic ratio given 85 minutes post anaphase onset  $\pm$  S.D, 2-tailed Student's T-test was used to assess significance across 4 independent experiments (\*); Ctrl,  $8.9 \pm 3.1$ , n = 174 ; CHMP2A siRNA  $5.4 \pm 2.6$ , n = 171, P = 0.0006; CHMP2A siRNA + CHMP2A<sup>R</sup>-FLAG  $8.4 \pm 3.3$ , n = 132, not-significant; CHMP2A siRNA + CHMP2A<sup>R</sup>-FLAG RRR-AAA  $5.4 \pm 2.2$ , n = 196, P = 0.0001).